The International Journal of Advanced Manufacturing Technology (2021) 112:1339–1358
https://doi.org/10.1007/s00170-020-06479-0

ORIGINAL ARTICLE

Parameterized multipoint-line analytical modeling of a mobile heat source for thermal field prediction in laser beam welding

Fabio Giudice [1] · Severino Missori [2] · Andrea Sili [3]

Received: 6 July 2020 / Accepted: 7 December 2020 / Published online: 3 January 2021

Abstract

The thermal effects of the "keyhole" full penetration welding mode, which is characteristic of high-power CO_2 laser, are simulated introducing a multipoint-line thermal source model based on heat conduction, parameterized by the distribution of the laser beam power, and the setting of the source system layout, and to be fitted on experimentally detected cross sections of the heat-affected or fusion zones of the weld. The proposed model allows to express the thermal field according to the moving reference system fixed on the overall heat source, and to analyze the temperature profiles that develop in some detection points fixed on the workpiece, as time varies during the welding process. By this way, it can be useful in evaluating the thermal effects that result from the variation of the main welding parameters (beam power, welding speed, plate thickness), with the aim of simplifying the selection of the optimal process conditions. As an application, reference is made to a cross section of a joint between plates of AISI 304 L austenitic steel. The fitting procedure allows to set the power distribution and layout parameters of the most suitable source combination (obtained by superposition of a line and two point sources). The value of the absorption coefficient also is assumed as fitting variable, so to overcome the complex problem of evaluating the beam power actually absorbed by the material on keyhole mode welding. Finally, the fitted model is applied to carry out a detailed thermal field analysis in the welded plates.

Keywords Laser beam welding · Keyhole · Analytical modeling · Thermal fields · Fusion zone

1 Introduction

In recent years, many finite-element models (FEM) have been developed to simulate the thermal profiles generated during welding, in order to have a valid means to properly predict, already during the design stage, the effects resulting from the choice of the various process parameters and evaluate the occurrence of any distortion and residual stress [1–3]. This allows to achieve particularly significant economic benefits in highly automated welding processes that require considerable initial investments, as in the case of laser beam. However, FEM simulations need increasing computational capacities and times, according to the degree of accuracy of the mesh in which the joint is divided, even if a certain simplification can be achieved by using 2D geometry [4]. Actually, in order to simulate the thermal flow in laser beam butt welding, even having a large calculation capacity available, simulation times are considerable [5].

Furthermore, these simulations have to be validated individually and this is usually carried out utilizing the results of experimental measurements which, by their nature, are to be considered specific to the particular welding conditions that are adopted [6]; therefore, the comparison with the thermal profiles obtained by analytical models are worth to be taken into account [7].

From the point of view of calculation, a less complex approach is based on considering directly the phenomenological laws of the heat conduction, utilizing the analytical solutions which can be developed starting from the equation proposed by Rosenthal in 1946 [8] and by the subsequent works of Carslaw [9] and Ashby and Easterling [10], which offered simulations of the temperature profiles generated by the advancement of

✉ Andrea Sili
asili@unime.it

[1] Dipartimento di Ingegneria Civile e Architettura, Università di Catania, 95123 Catania, Italy

[2] Dipartimento di Ingegneria Industriale, Università di Roma, Tor Vergata, 00133 Roma, Italy

[3] Dipartimento di Ingegneria, Università di Messina, Contrada di Dio, 98166 Messina, Italy

moving sources of various geometries, as it was shown also in a recent review by Mackwood and Crafer [11].

The major limitation of thermal conductivity-based models consists in neglecting the complex fluid dynamics phenomena that develop within the keyhole in high penetration laser beam welding, and which entail real thermal distributions that are very difficult to be modeled analytically.

To compensate for the simplification of the heat conduction modeling, the analytical approach proposed here is based on a parameterized multipoint-line model that allows to simulate the actual heat source generated by the keyhole, through combinations of virtual line-point sources. Their effects on melt pool and weld cross sections can be estimated and used to fit the model parameters (that define the distribution of source strength, and the layout of the source system), by comparison between analytical and experimental welding profiles (i.e., the melt cross section, or the heat-affected zone boundaries).

To show the application of the proposed model, reference is made to the case of plates of AISI 304 L austenitic steel, 10 mm thick, butt-welded by a single CO_2 laser beam pass, interposing the filler material in the form of consumable thin inserts, with reference to a process previously experimented [12, 13]. The full penetration keyhole mode was simulated through a line source along the entire thickness of the joint, which acts together with two point sources located respectively on the surface and inside the joint. The strength distribution and layout parameters of the analytical model were fitted on welded sections observed in an experimental joint between the plates.

The fitted model allows to analyze in detail the overall thermal field due to the moving heat sources that simulate the laser beam welding effects, also focusing on the temperature profiles that develop in fixed points on the workpiece, as time varies. Therefore, it can give the opportunity of evaluating the thermal effects resulting from the setup of welding parameters, such as the heat source power, the welding speed, and the plate thickness involved, considerably facilitating the selection of optimal process conditions, and the welding process control.

2 Materials and methods

2.1 Premises on thermal modeling for high penetration laser beam welding

For low-power laser beam welding, the laser light for the most part is reflected by the metallic material, while a limited portion of the beam energy is absorbed in a very thin layer at the surface of the workpiece by direct Fresnel absorption mechanism.

For high energy intensity beam, instead, vaporization of the metal surface occurs, forming a depression in the workpiece. As the depression deepens, the narrow cavity known as "keyhole" forms (Fig. 1), and the beam rays are scattered within the keyhole walls, partially absorbed on the surface and partially reflected towards a new point on the walls. This multiple Fresnel absorption/reflection phenomenon considerably increases the overall energy absorption, and results in high vapor pressure and temperatures. The metal vapor that fills the keyhole cavity damps the beam, absorbing partly the incoming laser light, that transmits kinetic energy to particles in the vapor. In the specific case of CO_2 laser beam (principal wavelength bands of about 10 μm), when the kinetic gain is significant, the ionization of the metal vapor (plasma) occurs, and some of the electrons become free, and absorb energy directly from the beam, increasing the plasma temperature and fostering the overall multiphysical mechanism that combine together laser-metal interaction, melting, vaporization, and plasma generation, and creates and stabilizes the keyhole.

As main result, the power of the laser source is absorbed at greater depths and more efficiently in the workpiece, allowing to obtain high weld penetration, and weld bead with high depth to width ratio.

It is also evident that the keyhole mechanism is based on a complex energy balance between laser beam, vapor, plasma, and melt pool, and the related fluid dynamic phenomena. Due to this reason, the most recent orientation of numerical modeling includes CFD (computational fluid dynamics) techniques [14]. However, the highly unstable process that governs it gives to the keyhole a dynamic behavior that involves considerable difficulties in modeling [15].

Keyhole modeling that neglects this aspect, and focuses on beam-matter interaction and conduction heat transfer, has the advantage of using the analytic solutions of the problem of thermal field due to moving heat sources, assuming the following conditions [8]:

- Quasi-stationary state—The heat source is moving with a constant speed along an axis of the solid. The axis is long enough, so the temperature distribution around the source becomes rapidly constant. As a consequence, an observer fixed to the source does not detect temperature changes around it as the source moves.
- Boundary conditions—The basic analytical solutions for the thermal field are referred to infinite medium. Particularly, to preserve the quasi-stationary state, the solid cannot be bounded by planes perpendicular to motion direction. This state condition instead can be considered maintained at semi-infinite and finite thickness, i.e. if the solid is bounded by one plane parallel to the motion direction, or if it is delimited within two planes parallel to the motion direction, respectively, assuming no heat loss through the bounding planes.
- Incident point source—The finite area of the real source is not taken into account, so the thermal field model leads to

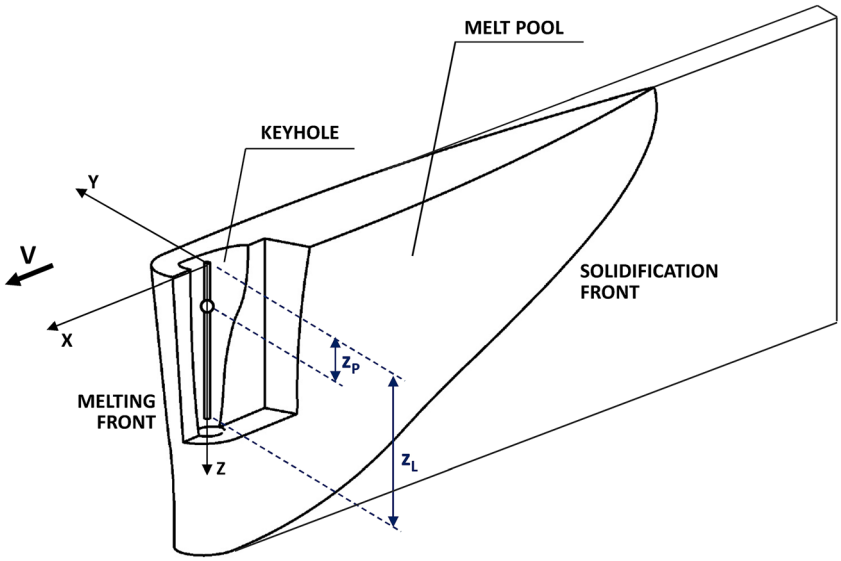

Fig. 1 High penetration laser beam welding reference scheme

infinite temperatures at the source, resulting in a lack of accuracy in the region where the heat source is incident.

Under these conditions, two fundamental solutions of the thermal field can be obtained from the general equation of conductive heat flow in a quasi-stationary state:

- Moving point source—It expresses the equation of a 3D field that can simulate a simple conduction welding approximated by a hemispherical shape.
- Moving line source—It expresses the equation of a 2D field co-axial to the line source that can simulate full penetration keyhole in solids of any thickness, or non-fully penetrating keyhole, depending on the depth of the source line inside the solid.

To overcome the limitations of these basic solutions, and model more effectively a keyhole welding, with particular regard to the typical "nail head" appearance at the top of the weld, combined point and line source model has been proposed, for workpieces of semi-infinite [16] and finite [17] thickness. Some adaptations and elaborations of the same model have been reviewed [18]. A complete overview on basic models for laser keyhole welding has been also proposed [19].

A keyhole model based on non-uniform line source has been proposed to obtain agreement between experimental and calculated fusion zone boundaries, and simulate thermal cycles at selected points for predicting the hardness in the heat-affected zone [20]. An approach based on a similar concept, with a line source whose strength varies with depth, has been also presented [6], correlating the temperature on the bottom surface with the penetration depth. Focusing on the real asymmetric keyhole profile, integrated point sources along curves, for both front wall and back wall of the keyhole, rather than along straight vertical lines, have been proposed [21]. As a further evolution of point and line source model, the temperature field in workpieces of semi-infinite thickness, under the influence of periodic point and line sources, has been formulated [22]. An alternative formulation for the steady-state heat conduction equation has been also proposed, using a prolate spheroidal coordinate system, and restricting the solution to the solid region outside the weld pool [23]. In more recent times, the analytical solution for a uniform heat source, derived from the solution of an instantaneous point heat source, has been used to investigate the effect of the temperature dependence of the material parameters [24]. Models based on alternative combinations of heat sources have been also proposed, such as double moving point source in semi-infinite solid [25], with the specific purpose of deriving the penetration and width of melting zone.

As already highlighted, the intrinsic limitation of these models based on thermal conductivity is to neglect the complex fluid dynamics phenomena that develop within the keyhole, and which entail real thermal distributions that are difficult to be modeled analytically. These distributions are the result of the interaction between various concurrent and coupled phenomena. The metal vapor that flows out of the cavity, being replaced by newly evaporated material, forms a plume which not only can participate to the beam damping [26], and cause defocusing, especially with CO_2 lasers [11], but also can create conditions of thermal concentration due to plasma radiation [16]. The plasma, in turn, plays a primary role in the stabilization of the keyhole, as it protects the keyhole cavity from cooling, and its radiation strengthens the vaporization at the keyhole surface; but as its temperature increases, due to further ionization of the metal vapor, and exceeds a critical value, beam damping effect becomes

dominant and vaporization breaks off [27]. All these effects, also conflicting with each other (damping, defocusing, thermal concentration), de facto determine an overall uneven thermal field, which will shape the cross section of the heat-affected and fusion zones of the weld.

2.2 Generalized multipoint-line model

The approach proposed here to compensate for the simplification of the heat conduction quasi-stationary hypothesis consists in superimposing a line source and multiple point sources. This approach can allow to simulate the non-uniformity of the overall thermal field generated by the keyhole, through a multipoint-line model, that is a combination of virtual line and point sources, whose theoretical effects on melt pool and weld sections can be estimated, and fitted by comparison with experimental welding profiles.

Under the conditions defined by Rosenthal [8] and previously summarized, considering a rectangular reference system (x, y, z), whose origin is fixed to the thermal source that moves along the x axis, and with the z axis directed along the thickness of the solid (Fig. 1), the two fundamental solutions of the thermal field that can be obtained from the general equation of conductive heat flow in a quasi-stationary state can be expressed as follows:

- Moving point source

$$T(x,y,z) = T_o + \frac{Q_P}{c\,\pi\,k\,r_P}\; e^{-\frac{v}{2\alpha}(r_P+x)} \tag{1}$$

It expresses the equation of the 3D field due to a point source, where T_o is the room temperature, Q_P is the point source strength (W), v is the heat source speed (m/s), k is the conductivity (W/mK), α is the diffusivity (m^2/s), and r_P is the radial distance from the heat source in the xyz space:

$$r_P = \sqrt{x^2 + y^2 + (z - z_P)^2} \tag{2}$$

being z_P the depth of the heat source location, with reference to the origin of the reference system, on the upper surface of the solid (Fig. 1).

In Eq. (1), the term c is a numerical constant: c = 2 for a point source on the surface of the solid ($z_P = 0$); c = 4 for a point source inside the solid ($z_P > 0$).

- Moving line source

$$T(x,y) = T_o + \frac{Q_L}{2\,\pi\,k}\; e^{-\frac{v}{2\alpha}x}\, K_0\left(\frac{v\,r_L}{2\alpha}\right) \tag{3}$$

It expresses the equation of the 2D field due to a line source along the z axis, where Q_L is the line source strength per unit length (W/m), K_0 is the zero-order modified Bessel function of the second kind, and r_L is the radial distance from the heat source in the xy plane:

$$r_L = \sqrt{x^2 + y^2} \tag{4}$$

This solution can simulate full or partial penetration keyhole on solids of any thickness, depending on the depth of the source line inside the solid z_L (Fig. 1).

Based on these analytical solutions, the multipoint-line model can be expressed by superposition of solution types expressed by Eqs. (1) and (3):

$$T(x,y,z) = T_o + \frac{Q_L}{2\,\pi\,k}\; e^{-\frac{v}{2\alpha}x}\, K_0\left(\frac{v\,r_L}{2\alpha}\right) + \sum_{i=1}^{n} \frac{Q_{P\,i}}{c_i\,\pi\,k\,r_{P\,i}}\; e^{-\frac{v}{2\alpha}(r_{P\,i}+x)} \tag{5}$$

where n is the number of point sources, $Q_{P\,i}$ is the strength of the ith point source (W), and $r_{P\,i}$ is the radial distance from the ith point source, expressed by

$$r_{P\,i} = \sqrt{x^2 + y^2 + (z - z_{P\,i})^2} \tag{6}$$

being $z_{P\,i}$ the depth of the ith point source location, with reference to the origin of the reference system; the numerical constant c_i in Eq. (5) is 2 or 4, if the ith point source is located on the surface of the solid ($z_{Pi} = 0$), or inside the solid ($z_{Pi} > 0$), respectively.

If P is the laser power (W), and η is the absorption coefficient, introducing the coefficients of power distribution γ_L and γ_{Pi} (being $\gamma_L + \Sigma\gamma_{Pi} = 1$), the strengths of the sources in Eq. (5) can be expressed by

$$Q_L = \gamma_L \eta\, P / z_L \quad Q_{Pi} = \gamma_{Pi} \eta\, P \tag{7}$$

and are constrained by the following condition:

$$\eta\, P = Q_L z_L + \sum_{i=1}^{n} Q_{P\,i} \tag{8}$$

Equation (5) allows to express the thermal field of multipoint-line model in each point of the space xyz, according to the moving reference system fixed on the overall heat source. To analyze the temperature profiles that develop in a fixed detection point on the workpiece, as time varies, i.e. as the distance of the mobile sources from the detection point varies during their movement, it is necessary to operate in all the terms of Eq. (5) that depends on the x coordinate, the following coordinate transformation:

$$x \rightarrow \xi = x - vt \tag{9}$$

where v is the moving speed along the x axis, and t is the time.

By means of this transformation, a fixed point on the workpiece, with respect to the mobile reference system xyz, is identified by the coordinates (ξ, y, z). In fact, considering (ξ', y', z') as the detection point:

- at $t = 0$ ($\xi' = x'$), that is at the beginning of the thermal analysis, the temperature $T(\xi', y', z')$ is calculated when the heat sources are positioned at the beginning of the translation along the x axis, and the point (ξ', y', z') is x' far from the heat sources along the x direction;
- at $t > 0$ ($\xi' = x' - vt$), the temperature $T(\xi', y', z')$ is calculated in the same point of the workpiece, when the heat sources have moved along the x axis of the quantity vt, and the point (ξ', y', z') is $x' - vt$ far from the heat sources along the x direction.

This setting in the analytical model allows to calculate also the cooling rate CR at the detection point (ξ', y', z'), as the heat sources move away along the x direction:

$$\mathrm{CR}(\xi', y', z') = \frac{\partial T(\xi', y', z')}{\partial t} \tag{10}$$

2.3 Model configuration and fitting

What has been introduced before is a multipoint-line heat source model, which is presented in a generalized formulation in order to be adapted to the peculiarities of each specific process to be analyzed. For this purpose, the generalized model must be configured and fitted to set up the virtual source system able to produce the same thermal effect of the actual keyhole mode laser welding on the workpiece during the specific welding process. This effect can be well expressed by the shape and width of the weld cross sections, which therefore can be taken as a reference for the configuration of the virtual heat sources, and for the fitting of the parameters that characterize it. The latter is as follows:

- the distribution coefficients of the laser's thermal power absorbed by the keyhole, i.e. the parameters (γ_L, γ_{P1}, …, γ_{Pi}, …) that define the strength distribution among the sources;
- the geometrical parameters of the heat sources, i.e. the length of the line source and the location depth of the point sources (z_L, z_{P1}, …, z_{Pi}, …), that define the layout of the model.

After establishing the composition of the heat sources that best represent the overall thermal field, these parameters must be fitted on the experimental profiles of the weld bead (i.e., the melt cross section, or the HAZ boundaries) on the plane orthogonal to the direction of source movement, to fully define the multi-source thermal model that can simulate the experimental bead.

By means of this phenomenological approach, the generalized model is adapted to the specific case to be analyzed, on the basis of features experimentally detected (the geometrical properties of bead cross section), in order to simulate the factual thermal effect of the keyhole without evaluating its complex energy-transfer processes. By varying the configuration of the model, it is possible to simulate an overall thermal source capable of determining the laser welding beads of the most common shapes: Those typical of deep penetration laser welding can be obtained by a basic combination of point-line sources [16]; those characterized by partial penetration can be obtained by the same basic combination, limiting the extension of the line source along the direction of the weld depth, and adding a point source at the end. By properly setting the configuration, it is possible to extend the model to the case of welds with low penetration factor and parabolic cross-sectional beads, combining only two point sources [17].

The purpose of the configuration, however, is to predetermine a system of heat sources so as to be able to produce as accurately as possible the experimental profile associated with the welding process to be analyzed. It is therefore advisable to prefix the most detailed and complete combination of the sources that best adapts to the shape of the weld bead profile, by coupling to the line source all the point sources that are deemed necessary to determine thermal fields capable of generating the shape features of the real bead profile obtained by the welding process. In all cases, whatever the number of sources, the power balance constraint expressed by Eq. (8) must be respected.

Then, the multi-source model, set up by the chosen combination of heat sources, will be defined in detail by fitting, on the shape of the bead cross section experimentally detected, the parameters that characterize the geometric layout and strength of the sources. In carrying out this operation, two fundamental issues must be considered:

- In the construction of the theoretical bead profiles obtained by the analytical model, as the parameters to be fitted vary, it is necessary to take into account the effect of the movement of the thermal sources at the welding speed. It produces a melt pool, and more generally a distribution of the isothermal surfaces of the thermal field, with typically shapes elongated by a rear trail, which develops in an orthogonal direction to the weld bead cross sections. This effect, and its outcomes on the construction of the theoretical contours of the fusion zone, will be made evident in the application described in the following Section 3.
- To fit the thermal model on a specific experimental profile of the weld bead could lead to a general inaccuracy of the model in calculating the thermal field in regions of the workpiece not strictly close to the cross section considered for the experimental detection of the bead profile. This is

due to the fluctuations in the cross-sectional profile of the melt pool along the welding line. An evaluation of these fluctuations, and of their effects on the thermal field calculated by the model, is necessary to evaluate the robustness of the model fitted on a single experimental profile, and therefore the significance of its results.

Finally, in principle, the heat source configuration could also be included in the fitting, using a large number of superimposed thermal sources, and leaving the fitting algorithm with the task of distributing the strengths of the sources in order to minimize or even cancel the superfluous ones, and enhance the necessary ones, depending on the peculiarities of the profile to be fitted.

This approach, entirely based on the mathematical operation of fitting the theoretically built curves on the experimental profiles, would extend the space of the fitting solutions: The greater the number of variables, the higher the number of potential solutions to the problem, to the detriment of the uniqueness of the final thermal model.

For this reason, and based on the results obtained and discussed in the following sections, some advices are considered convenient for configuration setting and final experimental fitting:

- Preliminarily to the fitting, proceed with a configuration of the thermal sources of the model based on qualitative criteria, taking into account the typical geometric properties of the two types of sources: The line source allows to model the most regular tracts of the experimental profile, with stable width along the depth of the weld; the point sources, which generate circular thermal fields (in 2D section planes), allow to model the tracts of the welded profile characterized by convex shapes, with significant increases in width.
- Set up the model limiting the number of heat sources to those strictly necessary to simulate thermal fields capable of producing the most marked characteristics of the shapes of the experimental profiles. An excessive level of detail in building the virtual source system, as well as limiting the effectiveness of fitting the geometric parameters and strength of the sources, is useless from the point of view of the evaluation of the thermal field on the workpiece. The latter, in fact, has a limited sensitivity to small variations in the shape of the experimental weld profile, as will be seen in the discussion of the application.
- Considering the type of optimization problem that the fitting algorithm has to solve, in which an absolute optimum is unlikely to occur, it may be considered advisable to use evolutionary algorithms, which are able to effectively manage the search for relative optimal solutions. In this case, however, the stability of convergence to substantially similar solutions must be assessed, in order to verify that the solution identified for a specific fitting, even if it is not unique from a strictly mathematical point of view, appears to be unique from the point of view of the thermophysical effect, which is the aspect of interest here.

2.4 Process setting and materials

Welding trials were performed by a laser beam traveling along a horizontal line, over the stationary workpiece in horizontal position (Fig. 2a). The laser source was a CO_2 device (type United Technologies - USA), which was equipped with a non-polarized multimode unstable resonator (maximum power of 25 kW) and operated in robotic style through a computer-controlled five axis gantry portal. The optical device consisted of a parabolic mirror, made of copper and water cooled, with a focal length of 682 mm. The laser beam was directed on the surface of the plate with a focus depth Δz = 5.5 mm and a spot diameter of 500 μm. The damaging effect of an excess of plasma, due to the ionization of metal vapor, is limited by a helium flow coming from a gas nozzle (internal diameter of 4 mm), which is directed over the molten bath in order to stabilize the keyhole. The use of helium, although more expensive than argon, is justified by its greater resistance to ionization.

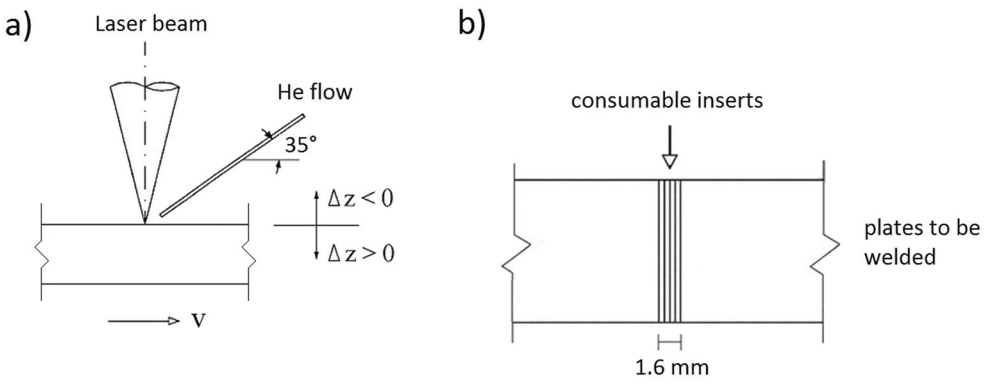

Fig. 2 Welding setup. **a** Longitudinal section (*zx* plane). **b** Cross section of the square-edged plates with the interposed consumable inserts (*xy* plane)

Table 1 Welding parameters

Laser beam power (kW)	Welding rate (m/min)	Laser spot diameter (μm)	Focus position Δz (mm)	Helium flow rate (l/min)	Filler metal inserts
14	1.2	500	5.5	20	No. 4 strips, each one 0.4 mm thick

Two plates, each one having size of 1000 × 1000 mm^2, 10 mm thick, were butt-welded with square edge preparation, no gap and filler metal in form of four consumable inserts, that were interposed between the edges (Fig. 2b) and initially fixed by gas tungsten arc tack welding.

It is well known that consumable inserts are often utilized for better fit up and easier root welding of those components that cannot be back welded. This procedure, previously experimented by the authors [28], was chosen for several reasons: It is easier to perform than using wire filler metal and allows to achieve geometrically regular weld beads, because it increases tolerance towards any geometric imperfections in the edge preparation or deviations of the beam alignment with respect to the welding axis. Moreover, utilizing the correct number of strips, the risk of incomplete fusion can be prevented easier than in case the filler metal is fed as wire. By this way, satisfactory joints have been obtained in [13] also from the point of view of lack of defects and final microstructure composition. The welding parameters are shown in Table 1.

The base material consisted of the austenitic stainless steel AISI 304 L, which is characterized by a high weldability due to its very low carbon content (Table 2).

A filler material was utilized, a Ni-based alloy, type AWS 309 L, in the shape of a packet of strips, each one 0.4 mm thick (1.6 mm total width of the insert along the y direction); the filler metal composition is given in Table 3. The choice of this filler material allowed to achieve, in the weld metal, a fully austenitic microstructure with a contour easily distinguished from the base material.

3 Model application

3.1 Visual and macrographic inspections of the experimental welds

Visual and macrographic inspections showed sound welds with complete penetration along all the plate thickness, without lack of fusion; moreover, the welds were free from cracks and other macroscopic defects. A representative macrograph of the welded section that will be considered for the thermal analysis fitting, obtained at the center of the welding line, and henceforth referred to as welded section 0, is shown in Fig. 3, with the relief of the contour of the fusion zone. It has a regular shape almost rectangular (about 2 mm wide), which becomes wider near the surface exposed to the laser beam, and presents an enlargement in correspondence with the position of laser focus.

3.2 Configuration and fitting of the analytical model

To define the layout and strength distribution of the analytical multipoint-line model that can create a theoretical welding section as similar as possible to the experimental one in Fig. 3, the following procedure was performed:

- Considering the non-particularly complex shape of the experimental welded section 0, the model was set as the superposition of a line source and two point sources, so referring to Eq. (5) in the formulation for $n = 2$: The line source extends for the entire thickness of the plate ($z_L = 10$ mm); the two point sources are placed in correspondence with the original surface of the plate ($z_{P1} = 0$ mm), to simulate the thermal concentration that creates the "nail head," and at the laser focus location ($z_{P2} = 5.5$ mm). In this setting, therefore, the layout parameters of the model are fixed in advance. The strength distribution parameters (γ_L, γ_{P1}, γ_{P2}), instead, will be fitted on the experimental profiles of the weld, under the constraint of power balance expressed by Eq. (8).
- The absorption coefficient η, constrained to the strength parameters and beam power by Eqs. (7) and (8), was considered a further fitting variable. This was done to evaluate the possibility of using the fitting of the model on the experimental welding profiles also in order to solve the complex problem of evaluating the power actually absorbed by the material, excluding the fractions absorbed by the plasma, and dispersed outside the keyhole.

Table 2 Base material composition

Base material	Plate thickness (mm)	C	Mn	Si	P	S	Ni	Cr	Fe
AISI 304 L	10	0.018	1.15	0.41	0.025	0.001	10.1	18.4	Bal.

Table 3 Filler metal composition

Filler metal	Insert total width (mm)	C	Mn	Si	Mo	Ni	Cr	Fe
AWS 309 L	1.6 mm	0.01	1.65	0.33	0.47	12.4	24.5	Bal.

- To construct the 3D model of the melt pool analytically, Eq. (5) was used to plot the isothermal curves corresponding to the solidus temperature T_S = 1673 K, on planes parallel to xy, varying depth z. In Fig. 4, the melt pool is constructed by the solidus isothermal curves for $z = 0, 2, 4, 6, 8, 10$. To obtain these curves, the values of AISI 304 L thermophysical properties reported in Table 4, estimated for the average temperature between room and solidus temperatures (700 °C), have been used in Eq. (5). The diffusivity α has been calculated as $k/\rho C_p$.
- Due to the effect of the movement of the thermal sources on the shape of the melt pool, as anticipated in the Section 2.3, the theoretical contours of the fusion zone have been obtained by the projection of the line of y maximum extension of the melt pool on a plane orthogonal to the welding direction x (Fig. 4). This is necessary because the contours of the fusion zone are the result of the solidification following the passage of the melt pool along the welding direction, and therefore are shaped by the maximum extension footprint of the melt pool on a yz plane.
- The fitting of the theoretical contours has been optimized by minimizing the sum of the squared distances on the y direction, between the experimental and the theoretical contours, calculated for both opposite profiles ($+y$ and $-y$) at four different depths along the z axis, drawn by dashed lines on the experimental profile in Fig. 5. The four depths have been distributed along the z axis taking into account two basic criteria: The upper and lower ends of the joint have been excluded, being the regions to which correspond particular irregularities of shape, combined with the greater deformation on the plates; the choice of depths that identify the comparison points between the theoretical and experimental curves must be wise, in order to detect the most significant morphological characteristics of the experimental profile on which to fit the analytical model. The fitting has been performed by the evolutionary solving tool implemented in Excel, showing a uniform convergence to stable solution, also as the main evolutionary parameters change (population size, mutation rate, seeding factor), and obtaining the result shown in Fig. 5. The overall set of parameters that define the model, distinguishing between the layout parameters (z_L, z_{P1}, z_{P2}) fixed in advance, and the fitted strength distribution parameters (γ_L, γ_{P1}, γ_{P2}) and absorption coefficient (η), is reported in Table 5, with the corresponding values of points and line source strength calculated by Eq. (7).

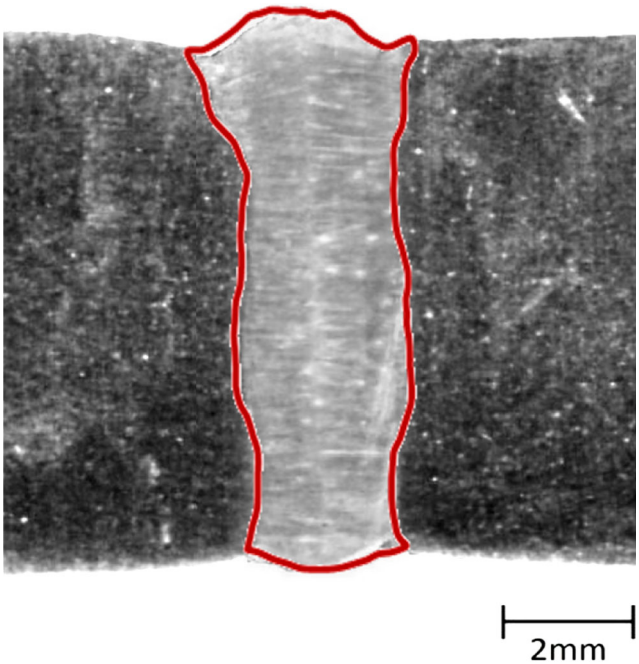

Fig. 3 Macrograph of the welded section 0 considered for thermal model fitting and relief of fusion zone contour

3.3 Model robustness and validation

It is reasonable to expect that the model fitted on a specific experimental profile of the weld bead can allow to calculate, with a high level of accuracy, the thermal field on the workpiece in a neighborhood of the same welding cross section on which the profile was detected. The same cannot be taken for granted with regard to regions of the workpiece not strictly close to the cross section considered for the experimental detection of the fitted bead shape, because of the fluctuations in the cross-sectional profile of the fusion zone, along the welding line. Significant variations in the shape of the bead section would lead to think that a model fitted on one section is not reliable in correspondence to other sections.

As already suggested in Section 2.3, to estimate the impact of the non-uniformity of the cross-sectional shape of the fusion zone on the model accuracy, it is necessary to

- survey the variations of this shape along the welding line;
- evaluate how much these variations affect the parameters of the model to be fitted, and the corresponding thermal

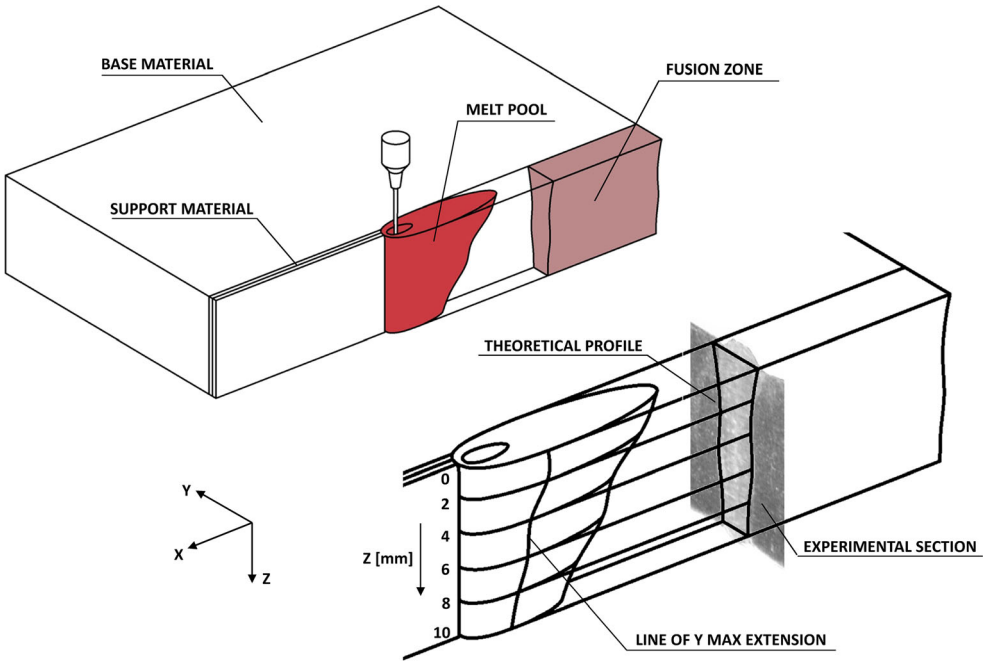

Fig. 4 3D modeling of melt pool and construction of theoretical contours of fusion zone

Table 4 Thermophysical properties of the AISI 304 L (700 °C) [29]

Density ρ (kg/m^3)	Specific heat C_p (J/kg K)	Thermal conductivity k (W/mK)	Diffusivity α (m^2/s)
7682	600	25	$5.42 \cdot 10^{-6}$

field, i.e. how much the thermal field described by the model fitted on a specific bead cross section, is sensitive to the fluctuations in the shape of the bead along the weld.

For this purpose, the detection of the experimental profiles of the welding sections was performed, as well as in correspondence to the weld midpoint (that is to the section 0

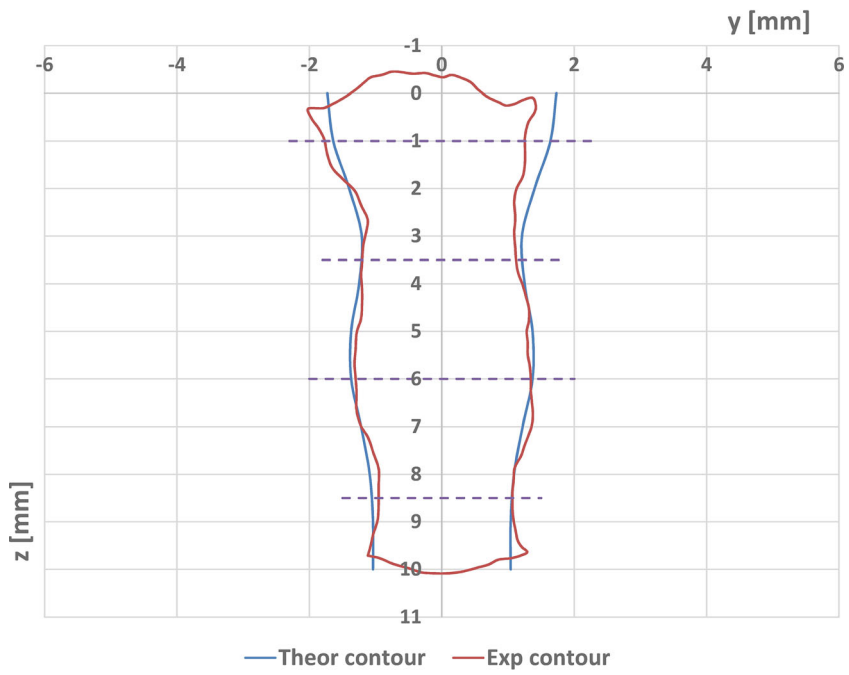

Fig. 5 Fitting between experimental and theoretical contours of the fusion zone (welded section 0)

Table 5 Setting of model parameters (fitting on welded section 0)

Layout parameters (fixed)		Strength distribution parameters (fitted)		Absorption coefficient (fitted)		Source strength (calculated)	
z_L	10 mm	γ_L	0.81	η	0.51	Q_L	577 kW/m
z_{P1}	0 mm	γ_{P1}	0.10			Q_{P1}	0.735 kW
z_{P2}	5.5 mm	γ_{P2}	0.09			Q_{P2}	0.629 kW

previously analyzed), also in correspondence to other four sampling points, arranged symmetrically with respect to the section 0, as shown in Fig. 6. The regions at the two ends of the welding line, more subject to process non-uniformity, have been excluded.

For each control section (1.1 and 1.2 on one side of the middle section 0, 2.1 and 2.2 on the opposite side), the theoretical profiles (in blue) were fitted on the experimental ones (in red) following the same procedure described above for section 0. The fitting of section 0 was reported in Fig. 6 for comparison. From a preliminary observation of the experimental profiles collected in the figure, a substantial similarity can be observed in the most marked morphological features. This is attributable to the high degree of automation of the laser welding process that favors the stability of the welding conditions, which translates into a tendency towards uniformity of the bead shape.

From the analysis of the fitted theoretical profiles, a prominent stability of them is found as the sampling section changes. This is confirmed by the values of the fitted parameters of the analytical model, reported in Table 6. It shows the values of the strength distribution parameters (γ_L, γ_{P1}, γ_{P2}), and of

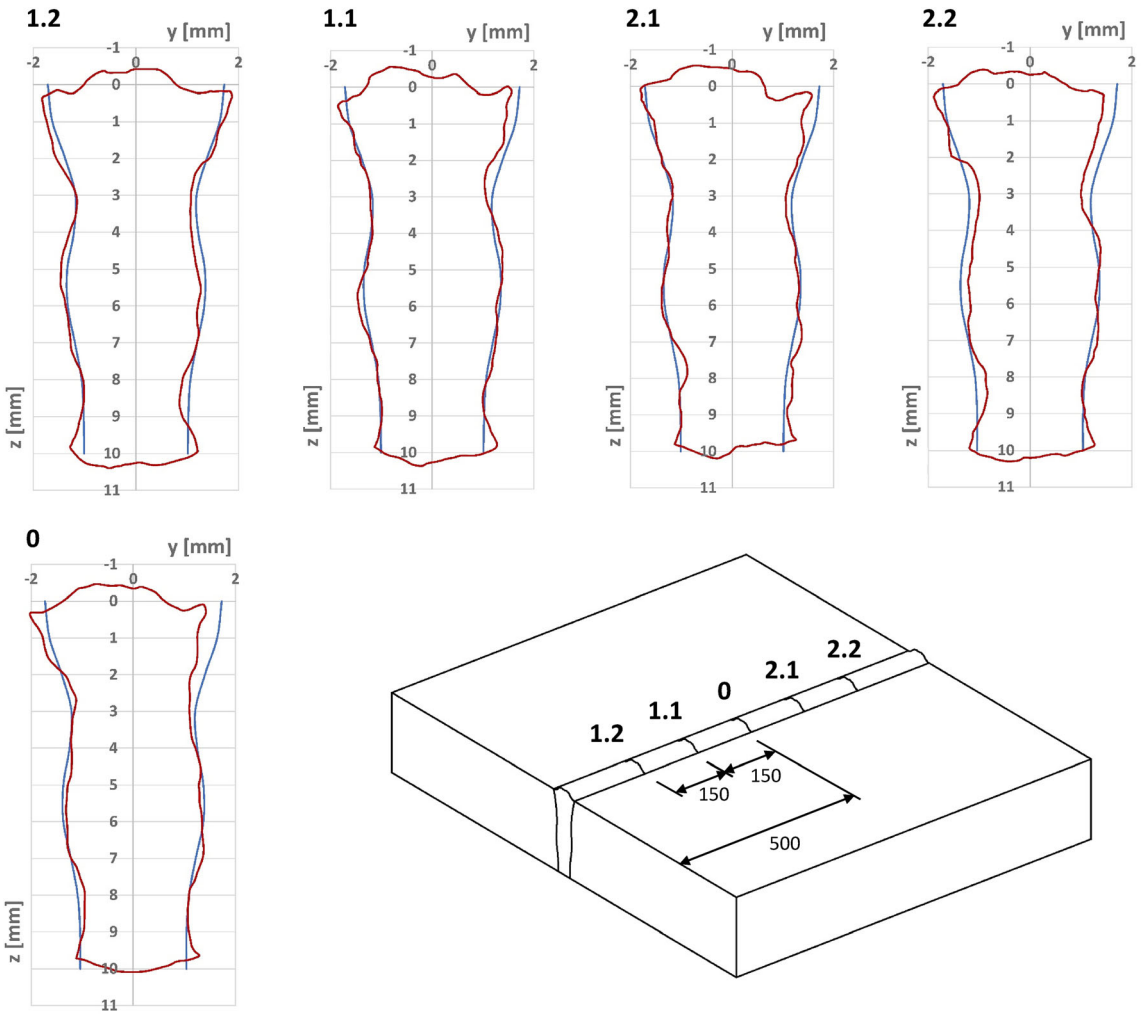

Fig. 6 Fitting between experimental and theoretical contours of the fusion zone (five sections along the welding line)

Table 6 Comparison and variability of model parameters with respect to the experimental fitting section

Section	0	1.1	1.2	2.1	2.2	Mean	St. dev.
γ_L	0.809	0.808	0.809	0.813	0.816	0.811	0.003
γ_{P1}	0.103	0.104	0.107	0.100	0.101	0.103	0.002
γ_{P2}	0.088	0.088	0.085	0.087	0.083	0.086	0.002
η	0.510	0.505	0.501	0.501	0.506	0.504	0.004
Q_L (kW/m)	577	571	567	570	578	573	5
Q_{P1} (kW)	0.735	0.734	0.747	0.704	0.715	0.727	0.017
Q_{P2} (kW)	0.629	0.626	0.594	0.608	0.590	0.609	0.018

the absorption coefficient (η), reported up to the third decimal place to highlight the slight variations. The low values of the standard deviation calculated for each of them confirm the limited variability.

The same table also shows the corresponding values of the source strengths (Q_L, Q_{P1}, Q_{P2}), calculated by means of Eq. (7). In this case, the variability is more consistent, but the effect on the calculation of the thermal field is in any case negligible. This is evident from the curves shown in Fig. 7. They are reported as a function of time, i.e. during the movement of the thermal source along the x axis with the velocity v. Each curve shows the thermal profile of a point located on the surface of the workpiece ($z = 0$ mm), fixed on the line orthogonal to the welding line and passing through its midpoint, for the time interval (25 s) necessary to complete the welding of the joint (for a remaining length of 500 mm, starting from the midpoint of the welding line to its end). The values of distance ξ (mm) between the detection point and the thermal source along the x axis, for each time t (s), are calculated using the coordinate transformation (Eq. 9), and also reported on the abscissa axis of the graph.

The curves are parameterized according to the y coordinate, which expresses the distance of each analyzed point from the welding line. For each point, the thermal profile has been calculated five times, once for each set of fitting parameters reported in Table 6, according to the variation of the experimental fitting sections taken into consideration in Fig. 6. However, the sensitivity of the thermal profiles with respect

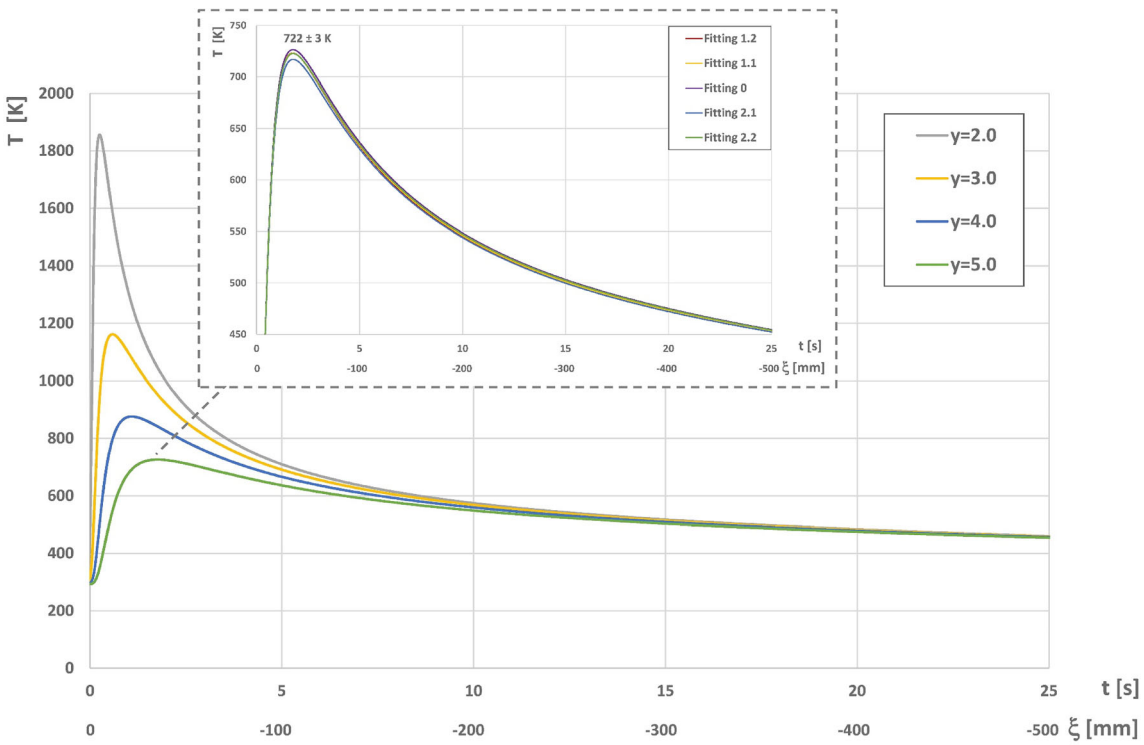

Fig. 7 Thermal profile of fixed points next to the welding midpoint, on the surface of the workpiece (at $z = 0$ mm), for the time interval (25 s) necessary to complete the welding, parameterized according to the y coordinate (distance of the point from the welding line)

to the fitting section is so low that, for each point analyzed, the thermal curves overlap. To appreciate the deviation, it is necessary to increase the scale factor, as done in the magnification shown in Fig. 7, for the point fixed at $y = 5$ mm: In this case, the maximum deviation that occurs at the thermal peak presents a variation of only ± 3 K with respect to the average value.

In this regard, it should be noted that the very fitting method proposed here plays in favor of the robustness of the analytical model with respect to the fluctuations of the experimental profile on which it is fitted. This method, detailed in the previous Section 3.2, is focused on the distances on the y direction between the experimental and the theoretical contours, calculated in relation to eight points (two points for each of the four different depths along the z axis, such as in Fig. 5). As a consequence, the fitting is sensitive to variations in the shape of the experimental profile localized near the comparison points, but it is not with respect to distant localized variations.

This observation confirms what has already been highlighted in Section 2.3 regarding the importance of choosing appropriately the comparison points between the theoretical and experimental curves, in order to detect the most significant morphological characteristics of the experimental profile on which to fit the analytical model.

To complete this part of the investigation, the thermal profiles calculated using the analytical model for the point at $y = 5$ mm, already highlighted in the magnification of Fig. 7, were used for model validation, by a comparison with a thermal profile experimentally detected on the same point. A K-type thermocouple was used for this purpose (chromel/alumel, tolerance class 2, temperature range between − 40 and 1200 °C, error 0.75%), and the result is shown in Fig. 8. The experimental profile (dashed red line) is delayed because of the thermocouple response time (time constant equal to 1 s), and appears to be in defect with respect to the theoretical estimate. The maximum error, corresponding to the temperature peaks, is equal to 7%; the error stabilizing towards the completion of the weld ($t = 25$ s) is equal to 6%. Considering the measurement error of the thermocouple, and the tendency of conductivity-based models to overestimate the temperature, as they neglect the other thermal transmission mechanisms and the related dispersion phenomena, the estimated error between theoretical model and experimental detection is limited, confirming the reliability of the analytical model and the accuracy of its thermal field simulations.

4 Results and discussion

4.1 Main results of model application

The search for the value of the absorption coefficient η included in the fitting of the model parameters was bound to a range of values (between 0.50 and 0.80), defined by minimum and maximum values available in the literature for keyhole mode laser welding of the steels [30, 31]. The high variability of this coefficient, which depends on a wide spectrum of factors, suggested to treat it as a constrained variable, which can also be fitted on the experimental profile of the fusion area. The value obtained (shown in Tables 5 and 6) is however validated by a theoretical calculation, set according to a model proposed by other authors [32]. According to this model, the fraction of laser beam absorbed by the material during the processes that take place inside the keyhole can be calculated as a function of some factors related to the geometry of the keyhole (mean keyhole wall angle, average path of the laser beam in plasma), and the plasma attenuation coefficient β. A value related to the welding speed has been set for the latter ($\beta = 130\ m^{-1}$) [33]. To set the other factors, the keyhole geometry has been simulated by imposing the boiling temperature at the keyhole walls [32], so to construct by means of Eq. (5) the

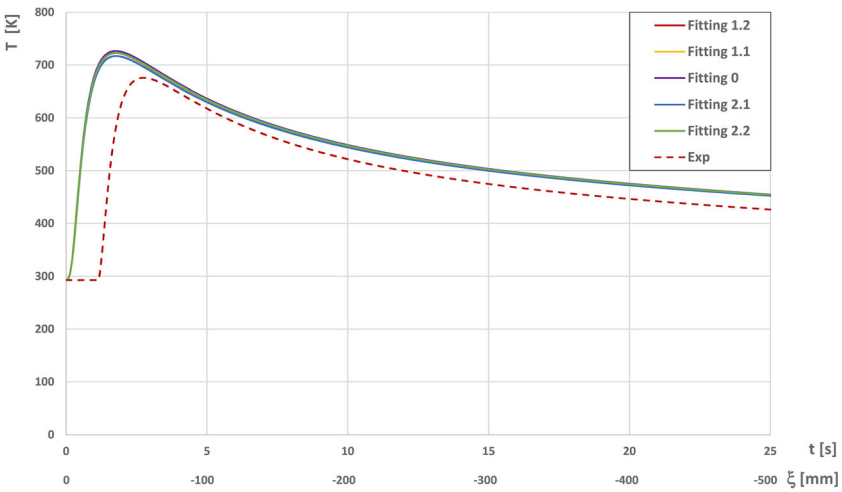

Fig. 8 Thermal profiles of the fixed point at $y = 5.0$ mm, on the surface of the workpiece (at $z = 0$ mm), for the time interval (25 s) necessary to complete the welding: comparison between theoretical and experimental profiles.

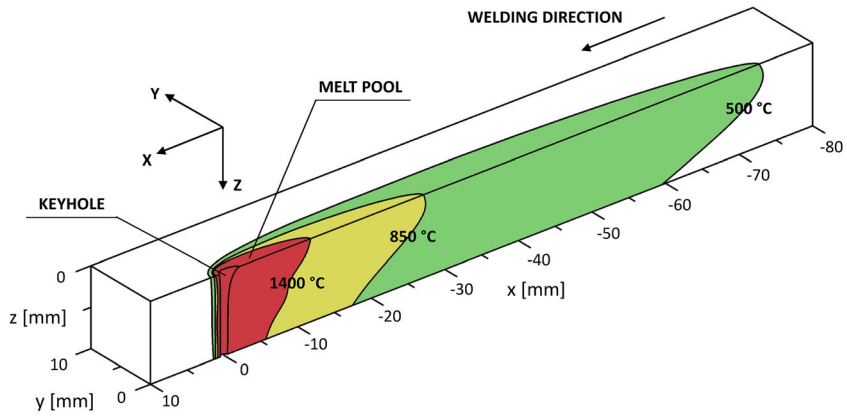

Fig. 9 3D simulation of the thermal fields: keyhole, melt pool, isothermals for 850 and 500 °C

corresponding isothermal surface. As a result, the value of 0.55 has been obtained for the fraction of laser beam absorbed by the material. Considering also that the calculation should concern only the portion of laser radiation that actually enters the keyhole, and that the wings of the radiation distribution have to be considered not intense enough to melt the material and reflected by the surface, a further 6-10% reduction in laser power must be considered for steels [30], thus obtaining a net absorption coefficient η estimated as between 0.49 and 0.52, therefore validating the result obtained by model fitting.

Once fitted on an experimental welding profile obtained by known process parameters, the proposed model allows to analyze the thermal field. In the case under consideration, the model parameters fitted on the welded section 0 (Table 5) were set in Eqs. (5) and (7), which allow to simulate different characteristics of the corresponding thermal field.

As it is known, the high energy density of the laser beam allows a deep penetration in a single pass. Overall, the amount of the heat supplied to the joint is very small when compared with the conventional arc welding processes. It produces a narrow weld with a reduced extension of the melt pool on the cross section, as confirmed by the following results of the thermal field analysis.

With reference to the welding conditions and the materials examined for the experimental investigation (Section 2.4), in Fig. 9, the following significative isothermal surfaces are simulated: the inner surface of the keyhole, assessed by imposing the boiling temperature of the AISI 304 L (~ 2800 °C) at the material-vapor interface; the melt pool, delimited by the isothermal surfaces corresponding to the solidus temperature (1400 °C); and the isothermal surfaces corresponding to temperatures of 850 and 500 °C, which is a critical range for sensitizing.

The equation of the 3D thermal field (Eq. 5) can also be used as if it were a two-variable function, fixing the third variable. Figure 10a shows the isothermal contours (1400 °C, solidus temperature) of the sections of the melt pool on the xy planes corresponding to different depths (z = 0, 2, 4, 6, 8, 10 mm) distributed along the thickness of the plates. Figure 10b instead shows the contours of the section of the melt pool on the welding plane (i.e., the xz plane for y = 0). In this case, the contours are the front and rear profiles of

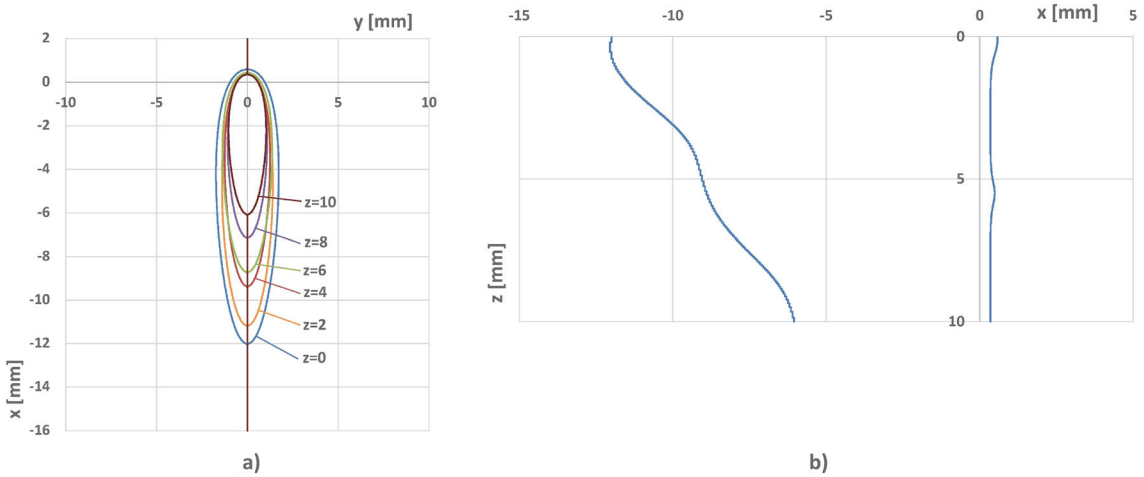

Fig. 10 Simulation of the melt pool. **a** Isotherms (1400 °C, solidus temperature) on the xy planes corresponding to z = 0, 2, 4, 6, 8, 10 mm. **b** Front and rear profiles of the melt pool on the xz plane at y = 0 (welding plane)

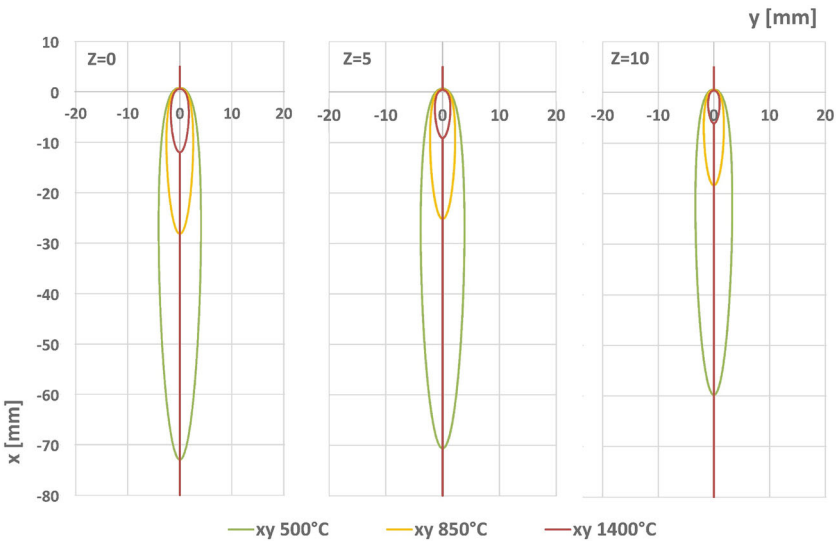

Fig. 11 Simulation of 1400 (solidus temperature), 850, and 500 °C isotherms at z = 0, 5, 10 mm

the melt pool on the welding plane. Figure 11 compares the isotherms of the melt pool (1400 °C) on the xy planes, with those at 850 and 500 °C, for z = 0, 5, 10 mm (i.e., on the upper and lower surfaces, and in the center of the plates).

In addition to the simulation of the overall thermal field generated by the moving thermal source, using Eq. (5) with the transformation of coordinates (Eq. 9), it is possible to analyze the thermal profiles on fixed points of the plates. In Fig. 12, the thermal profiles are calculated on the horizontal plane at the center of the thickness (z = 5 mm), as a function of y (distance of the point from the welding plane), and parameterized with the time, i.e. as the heat source moves away from the detection point during its travel along the x axis with the velocity v. This type of representation, therefore, allows to simulate the effect of the thermal source movement along the x direction, on points of the workpiece localized along a line parallel to the y axis.

The distance between the detection point and the thermal source, for each time t (s), is quantified by the corresponding value of ξ (mm) calculated using the coordinate

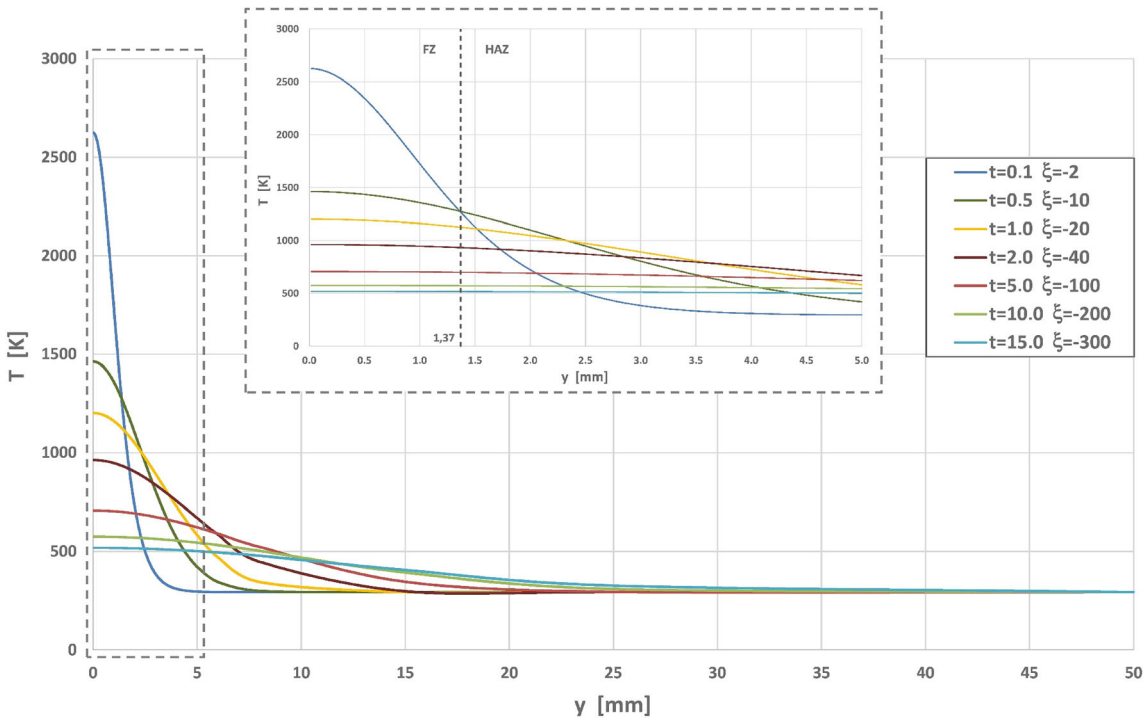

Fig. 12 Thermal profile of points on the initial welding edge until y = 50 mm, at z = 5 mm, parameterized according to the welding time, i.e. to the distance ξ from the heat source

transformation (Eq. 9). It can be noted that, for points that are more than 50 mm far from the welding plane, no thermal effect can be detected. In the same figure, the magnification of the y range from 0 to 5 mm highlights the thermal profiles in the region at the interface between the fusion zone FZ and the heat-affected zone HAZ (the point for $y = 1.37$ mm represents the FZ-HAZ boundary at $z = 5$ mm, which has been identified by means of the procedure shown in Fig. 4).

In Fig. 13, instead, thermal profiles of the same type of Fig. 7 are reported as a function of time, i.e. during the movement of the thermal source along the x axis with the velocity v. Also in this case, the values of distance ξ between the detection point and the thermal source, for each time t, are reported on the abscissa axis. Differently from Fig. 7, instead, here each curve shows the thermal profile of a fixed point on the initial welding edge, at the center of the thickness ($z = 5$ mm), for the time interval (50 s) necessary to complete the welding of the entire joint (extended for a length of 1000 mm). The curves are parameterized according to the y coordinate, which expresses the distance of the point from the welding plane. Among them, the point for $y = 1.37$ mm that represents the limit of the fusion zone at $z = 5$ mm is reported.

Also in this case, it can be confirmed that for points that are more than 50 mm from the welding line, no thermal effect is detected. In the same figure, the magnification of the time range from − 1 to 5 s shows that the theoretical thermal increase in a fixed point occurs just before the thermal source is in line with the detection point ($t < 0$), since the point already feels the effect of the front part of the thermal field, even if the latter is flattened with respect to the source axis (Fig. 9). For $t > 0$, i.e. as the thermal source moves away along the x axis, the point feels the extensive wake of the thermal field, and therefore has the most significant thermal profiles. This type of analysis is particularly useful for evaluating the exposure times of the points of the material at high temperatures, which can have significant effects on the HAZ, as for example in the case of stainless steels, which may be affected by the phenomenon of sensitization. In the present case, it is possible to establish that, due to the short exposure time (< 4 s) of all the points analyzed at the critical temperatures in the range 500-850 °C (773-1123 K), this metallurgical deterioration, typical of the austenitic steel, can be excluded [34].

4.2 Summary of key features and implications of the approach

In light of the application and the results obtained, a synthesis of the main peculiarities of the proposed approach to the modeling of thermal effects due to laser welding, and some significant implications, can be outlined.

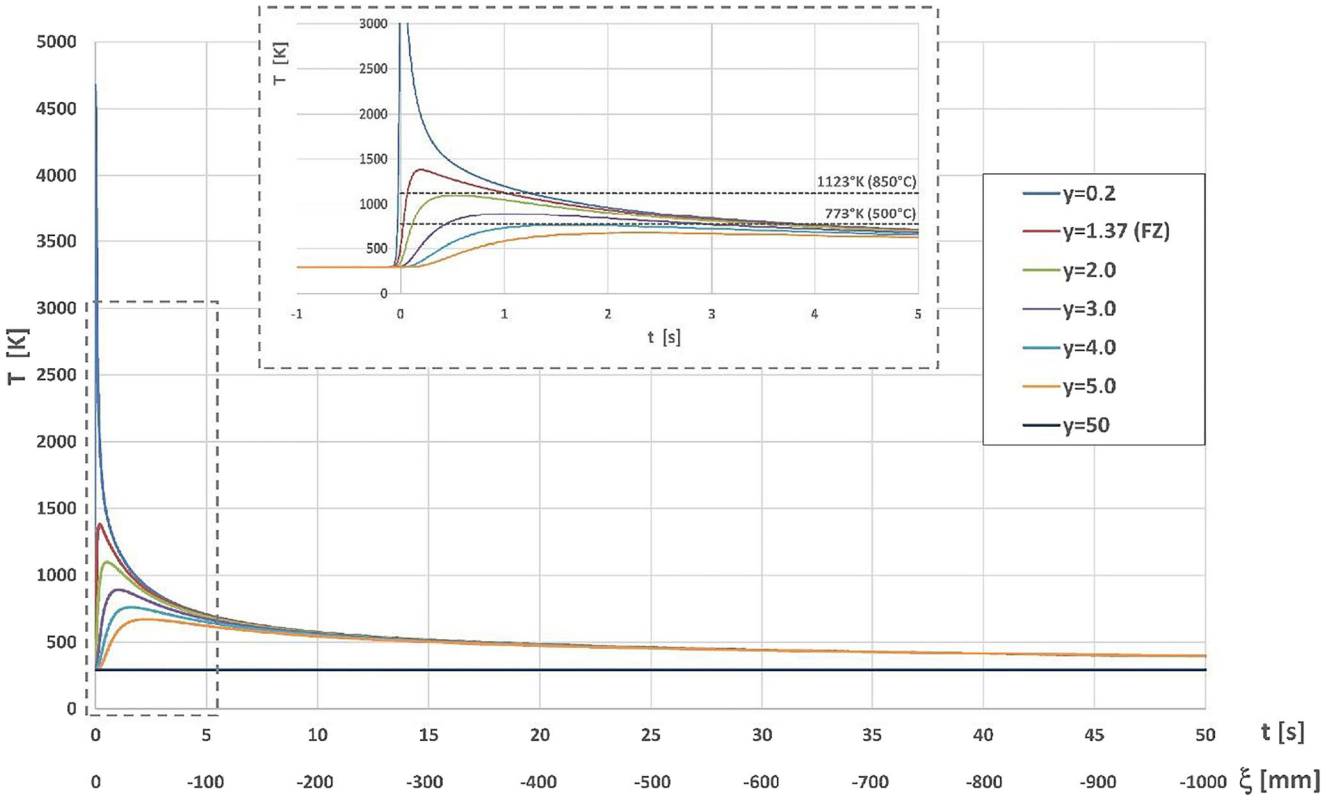

Fig. 13 Thermal profile of fixed points on the initial welding edge, at $z = 5$ mm, for the time interval (50 s) necessary to complete the welding, parameterized according to the y coordinate (distance of the point from the welding plane)

The following key features that characterize the approach differentiate it from the previous experiences on basic conductivity modeling of high penetration laser welding:

- Multi-source system setup and modulation—In the approach to basic conductivity modeling of high penetration laser welding, the observation of the experimental weld bead cross section usually constitutes a fundamental step for a qualitative preliminary choice of the heat sources to be used [16, 17, 19, 20, 25]. In the present case, the setting of the heat source system is generalized, and it can be modulated, starting from a specific concept: Use the combination of the sources that better adapts to the shape of the weld bead profile, by coupling a line source with all the point sources that are capable of generating the shape features of the real bead profile obtained by the welding process. Then, the detection of the experimental bead cross section is at the center of the fitting phase. In the case of the application described in Section 3, the preliminary configuration of the thermal source system was facilitated by the marked and clear features of the shape of the weld beam (substantially stable along the entire weld, as highlighted in Section 3.3), and by the detailed information on the process conditions (in particular the laser focus position). But, in principle, the heat source configuration can be entirely included in the fitting, so the proposed approach allows to use a theoretically unlimited number of superimposed thermal sources, leaving the fitting algorithm with the task of distributing the strengths of the sources in order to minimize or even suppress the superfluous ones, and enhance the necessary ones, depending on the features of the fusion zone profile to be fitted.
- Experimentally fitted model—As highlighted above, the experimental detection and observation of the bead cross section, as a precondition to set up the system of thermal sources that must simulate the global thermal effect of the beam-matter interaction, are well-established phases in the conductivity-based modeling of the keyhole effects on thermal field. Generally this observation is qualitative, and aims at the choice of heat sources to be used. In some previous works, it is explicitly suggested to configure the sources with regard to the experimental cross section. Nevertheless, approximated, not-strictly analytical fittings of a limited number of parameters are used, e.g. superimposing bundles of theoretical profiles, as the parameter to be set varies, on the experimental profile [16]. A clear overview on the results that can be obtained by this type of approach is shown for different shapes of the bead cross section [17]. In more recent experiences can be found hints to mathematical fitting [25], but also in this case the fitting is operated on a fixed and restricted number of parameters, and without indications on how the fitting was set up and optimized. The model proposed here can be considered an "experimentally fitted analytical model," with a fitting operation that is characterized by no limits on the number of parameters, by virtue of the generalization of the model; is theoretically capable not only of modulating the absorbed powers between the various sources, but also of combining in the most efficient way the distribution of source strengths with the geometric configuration of the entire system of sources, up to suppressing the superfluous ones, not suitable for representing the virtual model that determines the real bead cross section; allows to estimate the absorption coefficient in the source-matter interaction; is based on a clear sampling procedure in the comparison between theoretical and experimental profiles, the robustness of which is evaluated with respect to the fluctuations of the experimental profiles along the welding line; and is performed taking into account the types of optimization problem and solution space.
- Estimation of the absorption coefficient—In the use of the conductivity-based models that do not take into account the thermophysical phenomena that characterize the keyhole behavior, the absorption efficiency at the beam-matter interface cannot be directly assessed. As a consequence, often the question of absorption efficiency is overlooked, or indicative values known from the literature are used as absorption coefficient. In the proposed work, the approach based on defining the thermal system that causes the final welding effect (represented by the bead cross-sectional shape) considers appropriate to estimate also the absorption coefficient as a value congruent to the final effect. Therefore, it is included in the fitting of the model, and subsequently in a specific validation phase (which in the proposed case gave a very comforting result about the significance of its estimated value).

The approach, characterized by the key features just outlined, can give the opportunity of evaluating the thermal effects resulting from the setup of welding parameters, such as the heat source power, the welding speed, and the plate thickness involved, considerably facilitating the selection of the optimal process conditions, and allowing a proactive welding process control. Furthermore, the articulated analysis of the thermal field that can be performed, at both global and local levels, creates the prerequisite for a complete evaluation of thermal distortion conditions, which constitute one of the fundamental problems in the study of welding process effects.

With regard to keyhole effect modeling, it is essential to highlight what has been stated before: The analytical simulation of the keyhole mode laser welding, based on thermal conductivity modeling and experimental fitting, is focused on defining the virtual source system able to produce the same thermal effect on the workpiece due to the actual keyhole during the welding process. Therefore, the keyhole effects are not obtained directly, by the study and modeling of the

phenomena that characterize its thermophysical behavior, but indirectly, fitting a virtual model of heat sources that simulate the thermal field capable of producing the same weld bead obtained from the real keyhole mode welding. However, this approach allows to obtain a fairly accurate localization of the laser beam absorption, corresponding to the distribution of the heat source strength, and a quantitative assessment of the overall absorption coefficient, by means of the same experimental fitting of theoretical weld cross sections. The latter result is particularly significant, as this possibility of estimating the absorption coefficient allows to overcome the complex problem of evaluating the power actually absorbed by the material in keyhole mode laser welding.

The melt pool, delimited by the isothermal surfaces corresponding to the solidus temperature of the processed material, and other significant isothermal surfaces, can be constructed and studied accurately and in detail. Instead, as a consequence of neglecting the thermal and fluid dynamic behavior of the keyhole, the shape of the latter can just be estimated approximately, by imposing the boiling temperature at the keyhole wall, understood as the material-vapor interface, so to construct the corresponding isothermal surface. Although this simplified approach to keyhole surface simulation is used in literature [14], a modeling of this level should be considered indicative, and far from the significance of the models specifically focused on the main aspects of the complex keyhole behavior [15].

4.3 Contextualization and comparison to the state of the art

The presented approach to the modeling of thermal field due to high penetration laser beam welding should be considered belonging to the field of basic conductivity modeling: It uses the analytical solutions of heat conduction equation and excludes flow analysis and modeling of thermophysical mechanisms in the beam-matter interaction (beam and flow coupling, Fresnel absorption, vaporization, etc.) [14]; it also excludes the use of numerical resolution methods (finite-element, boundary-element, finite-difference methods) [11].

With reference to this specific field, some preliminary considerations on previous works emerge:

- They are set up for the primary purpose of making predictions on the distribution of power absorption, or correlating the absorbed power with the welding penetration, rather than developing a model for calculating as accurately as possible the thermal field to be extended to the workpiece. Detailed simulations of thermal cycles and experimental validation of these results through thermal measurements are occasionally reported.
- Although these models are all based on the observation of the bead cross section, and in some cases they are expressly configured with reference to different types of shape of the melt cross sections, they are not arranged for an extended mathematical fitting on the experimental profiles of the weld bead.

The approach proposed here, on the other hand, is focused on the simulation of the thermal field, and uses the fitting on the real experimental profiles of the weld sections precisely to refine the model as much as possible. In setting up the work carried out, the latter aspect was considered fundamental: In order to define a virtual model of heat sources that overcomes the approximations inherent in the conductivity-based approach, neglecting the multiphysics phenomena associated with the keyhole behavior, it is necessary to configure and set it in order to produce the real effect of the welding process; this can be done by fitting the model on the experimental profiles of the weld cross section.

As an evidence of the preliminary considerations on works of the specific reference field reported above, in few of them the analysis of the thermal field is as detailed as the one proposed here, and is validated by thermal measures experimentally detected. From a qualitative point of view, it is possible to observe a congruency between the trends of the thermal profiles shown in Fig. 13 and similar profiles reported in literature [23]. Some results were presented in [20], to validate by experimental temperature measures the thermal cycle simulated in selected points of the workpiece as a function of time (i.e., during the movement of the sources along the welding line). A single non-uniform line source was used to simulate the keyhole thermal effect in full penetration welding on a low carbon steel. As results of the comparison between theoretical and experimental thermal profiles in some points, the theoretical profiles were congruent with the experimental ones after a certain welding time, as the heat source moves away from the detection point, while in the first part of the thermal cycle, when the heat source is closer, they present substantial deviations from experimental profiles: In the case of a fixed point at 5.0 mm from the welding line, a maximum error of about 50%, corresponding to the temperature peaks, is found. The error estimated in the case presented here (Section 3.3, Fig. 8), at the same distance from the welding line, is homogeneous during the entire welding time interval, and remains below 10%. The markedly different results in the first part of the thermal cycle appear reasonably attributable to a greater accuracy of the proposed model that is configured and fitted according to the method outlined before, if compared to simpler models.

4.4 Limitations and potential extension of the approach

The need of basic conductivity modeling for fitting on the experimental profiles of the weld cross section produces models which are characterized by a limited capacity in

predicting the welding bead shape. Furthermore, in principle, it restricts the validity of thermal field simulations to the process conditions that produce the cross-sectional profiles of the weld bead on which the model is fitted.

This limitation is intrinsic to the basic conductivity approach in analytical modeling, and consequently to all the models that are derived from it.

Also the proposed model is affected by the same limitation, which on the other hand is a strength of the approach set here: It makes the analytical model flexible and easily adaptable to the specificity of the case to be analyzed, and reliable in the prediction of the thermal field, as demonstrated by the application and results previously discussed in detail. The proposed model fitting on the experimentally detected weld bead is enhanced and evolves to a kind of "generation phase" of the virtual system that creates the real effect (that is the bead cross section). This "generation" in the most general cases consists in suppressing the sources that were preliminarily set up, but result unsuited to obtain the real thermal effect; locating the necessary sources; defining the distribution of the corresponding strengths; and setting the absorption efficiency most congruent with the final effect. As a consequence, two fundamental goals are achieved: to refine the model and make it fully able to describe the entire thermal field, even when the position of the thermal source varies over time, in an accurate and reliable manner (as evidenced in Section 3.3, by the estimate of the error with respect to the experimental detection of the temperature profiles); to allow the evaluation of the absorption efficiency at the beam-matter interaction, without resorting to complex multiphysical modeling and numerical resolution methods that, however refined they may be, still require some form of experimental validation (in Section 4.1, the fitted value of the absorption coefficient is validated too, by comparing it to the one estimated using a dedicated analytical model found in literature).

As final observations on the predictive capacity of the proposed model, it should be noted in advance that the possibility of using a model calibrated on a specific experimental condition, in relation to other process conditions, constitutes the main criticality even for the most advanced tools that are born with a greater predictive capacity, such as numerical models that simulate the various thermo-fluid dynamics aspects related to the keyhole phenomenon. Also for these tools, in fact, the need for extensive experimental data allowing to validate the simulated results remains the key issue [14].

Nevertheless, although this main limitation of the experimentally fitted models cannot be overlooked, it must be considered that a potential use of the proposed model under process conditions other than those on which it is fitted seems concrete and is worthy of further investigation.

The validity of the model fitted on experimental profiles produced by specific process parameters, in some cases, can be extended to other process conditions. This occurs when the variation of the process parameters is such as to induce effects on the morphological characteristics of the weld bead cross sections that fall within the robustness limits of the model. In this regard, it has been highlighted before how the proposed fitting procedure, and the measures recommended in its implementation, can limit the sensitivity of the model to the local geometric details in the shapes of the experimental welding sections. This occurs because the fitting is focused on the morphological characteristics more marked and peculiar of the experimental profiles (Sections 2.3 and 3.3).

In the more extended practice, at least one bead cross-sectional sample is necessary to fit the model on the real welding conditions. A data collection aimed at the correlation, by the type of joint and material, between the process parameters and the characteristics of the weld bead profiles, starting from the results already presented by other authors [35], can be a first approach to overcome this intrinsic limitation.

It seems particularly promising to perform an experimental campaign aimed at correlating the main process parameters (primarily laser power and welding speed) with the morphological features of the bead cross section. In fact, the model and the fitting procedure are suitable for correlating the process conditions with the parameters of the model by interpolating experimental results. This would substantially expand the simulation potential of the thermal field as the process conditions vary, and it is the focus of an ongoing research activity which will constitute the natural development of the work presented here.

5 Conclusions

A generalized heat conduction-based analytical model was developed to simulate the thermal fields produced in high penetration laser beam welding. The presented approach proposes to compensate for the simplification typical of the heat conduction quasi-stationary modeling, by simulating the actual heat source due to the keyhole mode, through a virtual heat source system, with the following features: It is configured by superimposing a line source and multiple point sources; it is parameterized by the distribution of the laser beam power between the virtual sources, and by the setting of the source system layout; it is conceived to be fitted on experimentally detected cross sections of the heat-affected or fusion zones of the weld, in order to obtain the most effective and reliable analytical model to simulate the thermal field corresponding to specific welding parameters.

For the model application and validation, reference has been made to a weld joint between plates of AISI 304 L austenitic steel, which was obtained by single pass CO_2 laser beam welding. A line source along the thickness and two point sources, located on the plate surface at the laser beam side, and inside the weld, where the beam is focused, have been

configured to constitute the overall heat source. By varying the strength distribution among the line and the two point sources, simulated contours of the fusion zone have been fitted on the experimental ones. As further result of the fitting procedure, a value of 0.51 for the laser's absorption coefficient has been achieved, in agreement with absorption modeling available in literature, overcoming the complex problem of evaluating the power actually absorbed by the material in keyhole mode laser welding.

The fitted model has been used for a thermal field analysis, in order to simulate the melt pool and some significative isothermal surfaces created by the moving heat sources, and the time-dependent thermal profiles on fixed points of the workpiece. The survey highlights how the proposed analytical approach allows a detailed evaluation of the thermal effects that result from the main welding parameters (beam power, welding speed, plate thickness), so to be useful in the efficient setting of process conditions and in welding process control.

Authors' contributions Fabio Giudice: conceptualization, methodology, data curation, writing—original draft, validation, formal analysis, visualization, and supervision.

Severino Missori: conceptualization, investigation, resources, data curation, and visualization.

Andrea Sili: conceptualization, methodology, data curation, writing—original draft, formal analysis, investigation, visualization, and supervision.

Data availability The raw data and processing aids required to reproduce the findings cannot be shared at this time as they form the basis for an ongoing study.

Compliance with ethical standards

Conflict of interest The authors declare that they have no conflict of interest.

Ethics approval Not applicable.

Consent to participate Not applicable.

Consent for publication Not applicable.

References

1. Syahroni N, Hidayat MIP (2012) 3D finite element simulation of T-joint fillet weld: effect of various welding sequences on the residual stresses and distortions. In: Andriychuk M (ed) Numerical Simulation - From Theory to Industry, edn., IntechOpen, chap. 24, pp 583–606. https://www.intechopen.com/books/numerical-simulation-from-theory-to-industry/3d-finite-element-simulation-of-t-joint-fillet-weld-effect-of-various-welding-sequences-on-the-resid
2. Islam M, Buijk A, Rais-Rohani M, Motoyama K (2014) Simulation-based numerical optimization of arc welding process for reduced distortion in welded structures. Finite Elem Anal Des 84:54–64
3. Sajek A (2019) Application of FEM simulation method in area of the dynamics of cooling AHSS steel with a complex hybrid welding process. Weld World 63:1065–1073
4. Nezamdost MR, Nekouie Esfahani MR, Hashemi SH, Mirbozorgi SA (2016) Investigation of temperature and residual stresses field of submerged arc welding by finite element method and experiments. Int J Adv Manuf Technol 87:615–624
5. Tomashchuk I, Bendaoud I, Sallamand P, Cicala E, Lafaye S, Almuneau M (2016) Multiphysical modelling of keyhole formation during dissimilar laser welding. Proceedings of the 2016 COMSOL Conference, October 12-14, Munich. https://www.comsol.it/paper/download/361001/tomashchuk_paper.pdf
6. Lankalapalli KN, Tu JF, Leong KH, Gartner M (1999) Laser weld penetration estimation using temperature measurements. ASME J Manuf Sci Eng 121:179–188
7. Anca A, Cardona A, Risso J, Fachinotti VD (2011) Finite element modeling of welding processes. Appl Math Model 35:688–707
8. Rosenthal D (1946) The theory of moving sources of heat and its application to metal treatments. Trans ASME 68:849–866
9. Carslaw HS, Jaeger JC (1959) Conduction of heat in solids. Oxford University Press, London
10. Ashby MF, Easterling KE (1984) The transformation hardening of steel surfaces by laser beam. Acta Metall 32:1935–1948
11. Mackwood AP, Crafer RC (2005) Thermal modelling of laser welding and related processes: a literature review. Opt Laser Technol 37:99–115
12. Missori S, Costanza G, Sili A, Tata ME (2015) Metallurgical modifications and residual stress in welded steel with average carbon content. Weld Int 29(2):124–130
13. Missori S, Sili A (2018) Prediction of weld metal microstructure in laser beam weld metal clad steel. Metallurgist 62:84–92
14. Svenungsson J, Choquet I, Kaplan AFH (2015) Laser welding process: a review of keyhole welding modelling. Phys Procedia 78:182–191
15. Volpp J, Vollertsen F (2016) Keyhole stability during laser welding-part I: modeling and evaluation. Prod Eng Res Dev 10:443–457
16. Steen WM, Dowden J, Davis M, Kapadia P (1988) A point and line source model of laser keyhole welding. J Phys D Appl Phys 21:1255–1260
17. Akhter R, Davis M, Dowden J, Kapadia P, Ley M, Steen WM (1989) A method for calculating the fused zone profile of laser keyhole welds. J Phys D Appl Phys 21:23–28
18. Dowden J, Kapadia P (1998) Point and line sources: models of power absorption in the theory of welding. Proceedings of ICALEO '98 Laser Materials Processing Conference, November 16-19, Orlando, Florida. https://lia.scitation.org/doi/abs/10.2351/1.5059194
19. Dowden JM (2001) The mathematics of thermal modelling: an introduction to the theory of laser material processing. Chapman & Hall/CRC, Boca Raton
20. Metzbower EA (1990) Laser beam welding: thermal profiles and HAZ hardness. Weld J 7:272 s–278 s
21. Kaplan A (1994) A model of deep penetration laser welding based on calculation of the keyhole profile. J Phys D Appl Phys 27:1805–1814
22. Dowden JM, Ducharme R, Kapadia PD (1998) Time dependent line and point sources: a simple model for time-dependent welding processes. Lasers Eng 7:215–228
23. Postacioglu N, Kapadia P, Dowden J (1993) A mathematical model of heat conduction in a prolate spheroidal coordinate system with applications to the theory of welding. J Phys D Appl Phys 26:563–573
24. Van Elsen M, Baelmans M, Mercelis P, Kruth J-P (2007) Solutions for modelling moving heat sources in a semi-infinite medium and

applications to laser material processing. Int J Heat Mass Transf 50: 4872–4882
25. Franco A, Romoli L, Musacchio A (2014) Modelling for predicting seam geometry in laser beam welding of stainless steel International. J Therm Sci 79:194–205
26. Mościcki T, Hoffman J, Szymański Z (2006) Modelling of plasma plume induced during laser welding. J Phys D Appl Phys 39:685–692
27. Zhou J, Tsai HL, Wang PC (2006) Transport phenomena and keyhole dynamics during pulsed laser welding. J Heat Transf 128:680–690
28. Missori S, Murdolo F, Sili A (2004) Single-pass laser beam welding of clad steel plate. Weld J 83:65 s–71 s
29. Mills KC (2002) Recommended values of thermophysical properties for selected commercial alloys. Woodhead Publishing, Cambridge
30. Hoffman J, Szymanski Z (2002) Absorption of the laser beam during welding with CO_2 laser. Opt Appl 32:129–145
31. Ricciardi G, Cantello M (1994) Laser material interaction: absorption coefficient in welding and surface treatment. Ann CIRP 43: 171–175
32. Rai R, Elmer JW, Palmer TA, DebRoy T (2007) Heat transfer and fluid flow during keyhole mode laser welding of tantalum, Ti-6Al-4 V, 304 L stainless steel and vanadium. J Phys D Appl Phys 40: 5753–5766
33. Myiamoto I, Maruo H, Arata Y (1986) Beam absorption mechanism in laser welding. Proceedings of Symposium on Laser Processing: Fundamentals, Applications, and Systems Engineering, November 12th Quebec City, Canada, vol 668, pp 11–18. https://www.spiedigitallibrary.org/conference-proceedings-of-spie/0668/1/Beam-Absorption-Mechanism-In-Laser-Welding/10.1117/12.938878.short
34. Weman K (2003) Welding processes handbook, vol chap. 14. Woodhead Publishing Ltd, Cambridge, p 143
35. Khan MMA, Romoli L, Ishak R, Fiaschi M, Dini G, De Sanctis M (2012) Experimental investigation on seam geometry, microstructure evolution and microhardness profile of laser welded martensitic stainless steel. Opt Laser Technol 44:1611–1619